An Experimental Study on Wave Energy Conversion Problem of Turbine-integrated OWC Chamber

Jeong-Seok Kim, Sewan Park, Gilwon Kim, Jiyong Park, Kyong-Hwan Kim, Bo Woo Nam, Su-Gil Cho, Chang Hyuck Lim and Seung-Ho Shin*

Abstract—**An oscillating water column-type wave energy converter (OWC-WEC) is a promising device for utilizing ocean wave energy resources. The OWC-WEC comprises a chamber structure and power take-off (PTO) system. The chamber converts the kinetic energy of the ocean waves into the heave motion of the internal fluid, which generates a reciprocating airflow. The airflow drives an air turbine and generator, and its rotational motion produces electrical energy. To investigate the energy conversion problem of the OWC-WEC, a model test was conducted using the turbine-integrated OWC chamber model in the two-dimensional wave flume. Since each energy conversion module of the OWC-WEC is driven based on their interaction, the chamber's fluid dynamics, the turbine's aerodynamics, and the rotor's dynamics are fully coupled during the energy conversion process. Therefore, the energy conversion characteristics of the OWC-WEC were discussed under various operational conditions based on the experimental measurements from the chamber, turbine, and servo motor.**

Keywords— **Energy conversion performance, Model test, Oscillating water column, Turbine-chamber interaction, Wave energy converter.**

I. INTRODUCTION

RECENTLY various energy extraction technologies have been developed to utilize abundant ocean wave energy resources. An oscillating water column-type wave energy converter (OWC-WEC) consists of a chamber structure and power take-off (PTO) system. An OWC chamber induces the oscillating fluid motion inside the chamber structure from the wave motion. An oscillating water column motion makes reciprocating airflow delivered to the PTO system. The PTO system comprises an air turbine, generator, and power control system. An airflow drives an air turbine and generator, and its rotational motion produces electrical energy. The movable part of the PTO system consisting of an air turbine and a generator set on a single shaft has the advantage of structural simplicity. Furthermore, the PTO system has the advantage in terms of reliability as it is isolated from the corrosion and direct hydrodynamic loads due to its above-water installation location [1,2].

During the energy conversion process, the OWC chamber and PTO system interact with each other and show coupled system responses [3]. Various experimental researches have been conducted to understand the

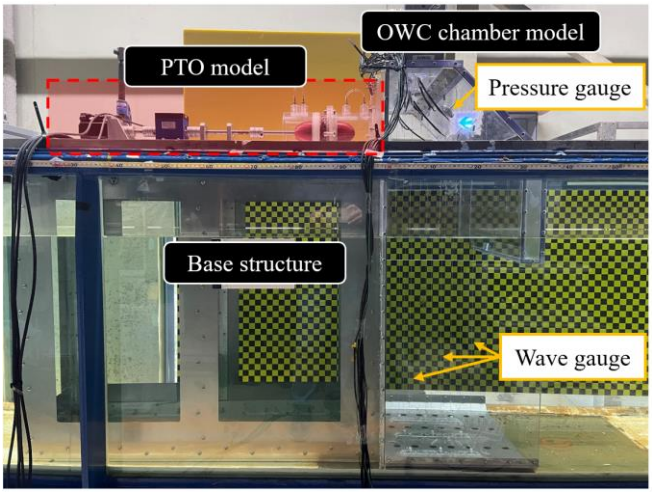

(a) Turbine-integrated OWC chamber model

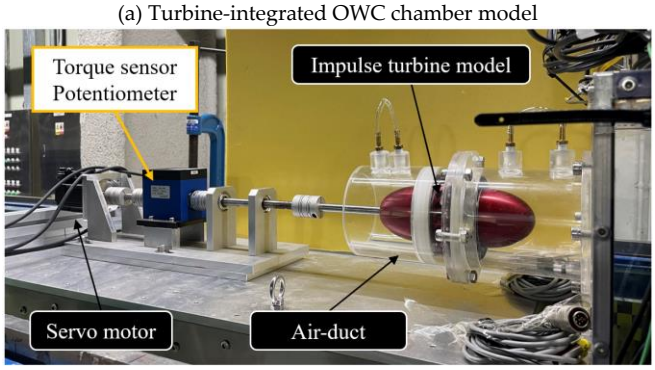

(b) PTO model

Fig. 1. Experimental set-up of the turbine-integrated OWC chamber model in the two-dimensional wave tank (KRISO).

This research was supported by the Korea Research Institute of Ships and Ocean Engineering (KRISO), a grant from Endowment Project "Digital platform development to support marine digital transformation" funded by Ministry of Oceans and Fisheries, Korea (PES4873).

Following authors are with the Korea Research Institute of Ships and Ocean Engineering (KRISO), 32, 1312 Yuseong-darero, Yuseong-gu, Daejeon 34103, South Korea. Their e-mail address is:

J.-S. Kim (jskim@kriso.re.kr), S. Park (sewanpark@kriso.re.kr), G. Kim (kimkilwon@kriso.re.kr), J. Park (jypark@kriso.re.kr), K.-H. Kim (kkim@kriso.re.kr), S.-G. Cho (sgcho@kriso.re.kr), C.H. Lim (ckdgur1092@kriso.re.kr), S.-H. Shin (shinsh@kriso.re.kr). B.W. Nam is with the Seoul National University, 1, Gwanak-ro, Gwanak-gu, Seoul 08826, South Korea (e-mail: bwnam@snu.ac.kr).

Digital Object Identifier: https://doi.org/10.36688/ewtec-2023-158

interaction mechanism between hydrodynamic and aerodynamic energy conversion [4,5]. The air turbine generates a pressure fluctuation, which suppresses the fluid motion inside the chamber. Since the mechanical torque and pressure fluctuation induced by the turbine depends on its aerodynamic characteristics, the control of the PTO system generates sequential effects on the rotor's dynamics, the turbine's aerodynamics, and the water column's hydrodynamics. Therefore, the energy conversion problem of the OWC-WEC needs to be investigated in conjunction with the entire system.

This study discussed the wave energy conversion problem of the turbine-integrated OWC chamber based on the model test in the two-dimensional wave tank. Various rotational speeds were considered to investigate the effect of the air turbine on the energy conversion performance. Furthermore, the nonlinearity in the energy conversion was tested under various wave height conditions. This paper is organized as follows; First, the experimental model and its set-up are introduced including the measuring sensors. Next, the experimental results and discussion are presented, and finally concluding remarks are provided.

II. EXPERIMENTAL DESCRIPTION

The model test for the turbine-integrated OWC chamber was carried out at the two-dimensional wave tank in the Korea Research Institute of Ships and Ocean Engineering (KRISO). The dimensions of the wave tank are as follows: length 25.6 m, breadth 0.56 m, and water depth 0.60 m. A piston-type wave maker and absorber were installed at the front and rear sides of the wave tank, respectively. Fig. 1 shows the configuration of the experimental model (black box) and measuring sensors (white box). The experimental model consists of a chamber structure and a PTO system. The chamber model was scaled based on Froude scaling with a ratio of 1/20 for the prototype OWC chamber structure and fixed on the bottom of the wave tank. The chamber structure model was made of acrylic plate and aluminum material. Three wave gauges were installed at uniform distance inside the chamber along the wave propagation direction to measure the internal water surface elevation. The measured internal surface elevation data was used to estimate the airflow velocity transmitted to the turbine model due to the difficulty in measuring the airflow velocity at the turbine-integrated air duct. The estimation method of the airflow velocity was verified based on the correlation test between the internal surface elevation and the airflow velocity measured by the hot-wire anemometer at the orifice based on the sub-experiment of the orifice-integrated OWC chamber model. The pressure gauge was installed at the top of the chamber model and measured the pressure fluctuation inside the chamber. As shown in Fig. 1(b), the impulse turbine model and supporting air duct were connected to the chamber model. The turbine model was connected to servo motors that controlled the turbine's constant rotational speed, which was measured by the potentiometer. The torque sensor is installed between the servo motor and the air turbine and measures the torque applied to the turbine by the airflow action. Table 1 shows the principal dimension of the prototype and experimental model. The sectional geometry of the prototype chamber structure corresponds to the Yongsoo Wave Power Plant located at Jeju Island in

TABLE I
PRINCIPAL DIMENSIONS OF EXPERIMENTAL MODEL

Items	Prototype	Exp. Model (1/20)
Water depth	12.0 m	600 mm
Chamber length	6.52 m	326 mm
Chamber width	11.4 m	570 mm
Skirt depth	1.3 m	65 mm
Skirt Thickness	1.1 m	55 mm
Duct Diameter	2.0 m	100 mm
Duct length	11.0 m	550 mm
Hub ratio	0.7	0.7
Hub length	1.52 m	76 mm
No. of blades	24	24
Turbine width	0.4 m	20 mm

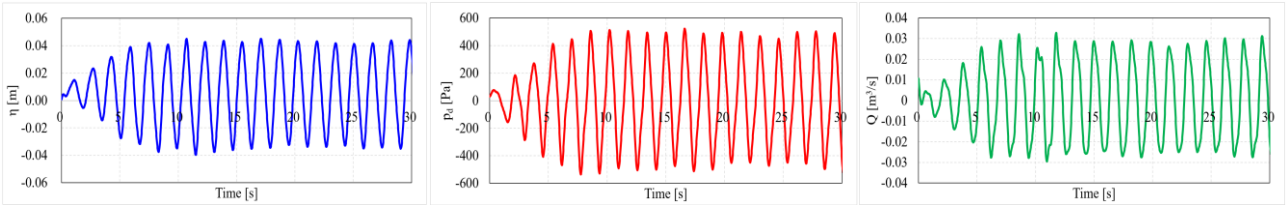

(a) OWC chamber

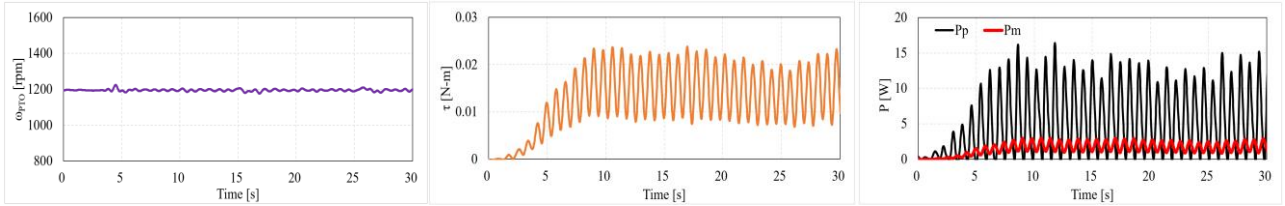

(b) PTO system

Fig. 2. Time-series responses of experimental model of the turbine-integrated OWC chamber under constant speed control (ω=1200 RPM) in regular wave (H=0.1 m, T=1.6 s).

TABLE II
EXPERIMENTAL CONDITIONS OF REGULAR WAVES AND TURBINE SPEEDS

T (s)	λ (m)	H (m)	H/λ	ω_{PTO} (rpm)
1.6	3.27	(H#1) 0.071	0.0217	400, 600, 800, 1000, 1200, 1400, 1600, 1800, 2200
		(H#2) 0.104	0.0318	
		(H#3) 0.140	0.0428	

South Korea.

Fig. 2 shows the measured data from the turbine-integrated OWC chamber model under the regular wave condition. Here, η, p_d, Q, and p_p correspond to the chamber responses, i.e., the internal water surface elevation, pressure drop, airflow rate, pneumatic power. Also, ω_{PTO}, τ, and p_m indicate the turbine responses, i.e., rotational speed, mechanical torque, and mechanical power of the turbine, respectively. Measured signals were obtained at a data acquisition device with a sampling frequency of 50 Hz and were analyzed to get the mean amplitude and mean power from the time series data under the periodical quasi-steady state by applying a zero-up crossing method. The average value of the measured data for 0.5 seconds was output for the measured mechanical torque due to the characteristics of the torque sensor.

Table II shows the experimental conditions for the regular waves and the turbine's rotational speeds. We consider the single wave period for the three wave height conditions. The incident wave defined from the measured surface elevation data at the location of the experimental model in the wave tank without the model. Furthermore, the experimental turbine model was controlled to various rotational speeds for each wave condition to examine the effect of the turbine operation on the energy conversion performance. A servo motor was utilized to rotate the air turbine at a constant speed. The servo motor was dynamically controlled in real-time by feedback on the difference between the target rotational speed and the measured value.

III. RESULTS AND DISCUSSION

A series of model tests for the turbine-integrated OWC chamber was conducted in two-dimensional wave tanks considering various regular wave heights and the turbine's rotational speeds. During the regular wave, a servo motor rotated the air turbine at a constant speed.

Fig. 3 shows the normalized amplitudes of the upward and downward surface elevation inside the chamber under various speed conditions. Here, the red line (H#1), green dashed line (H#2), and blue dashed-dotted line (H#3) indicate the three different wave height conditions. A and ω are the amplitude and angular frequency of the incident wave. The water surface motion decreased as the rotational speed of the turbine increased, which can be attributed to the turbine-oriented pressure suppressing the internal surface motion. Besides, when the airflow is discharged, the RAO of upward surface motion tends to decrease gradually with increasing wave height, as shown in Fig. 3(a). It means that the pressure generated by the turbine significantly affects the water column inside the chamber as a damping force. Furthermore, the increase in wave height induces a nonlinear pressure increase related to the aerodynamics of the turbine, so the water column motion RAO shows a wave height dependence. As shown in Fig. 3, the motion of the fluid inside the chamber exhibited vertical asymmetry, with the amplitude of the upward motion being greater than that of the downward motion. However, the RAO of the downward motion showed a different trend from the RAO of the upward motion under the H#3 condition.

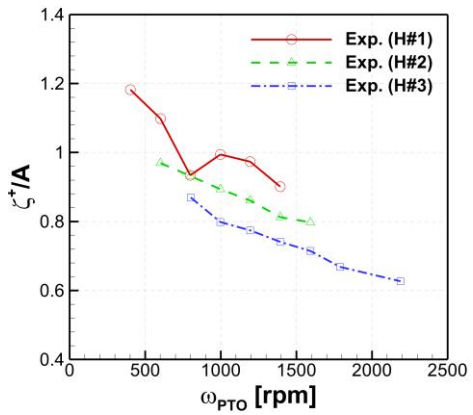

(a) Upward surface motion

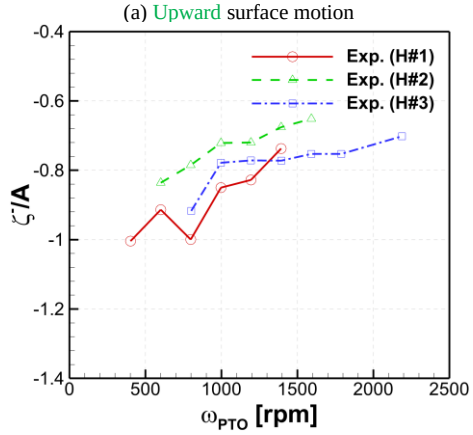

(b) Downward surface motion

Fig. 3. Surface motion RAO inside the OWC chamber under various wave heights and turbine's rotational speeds.

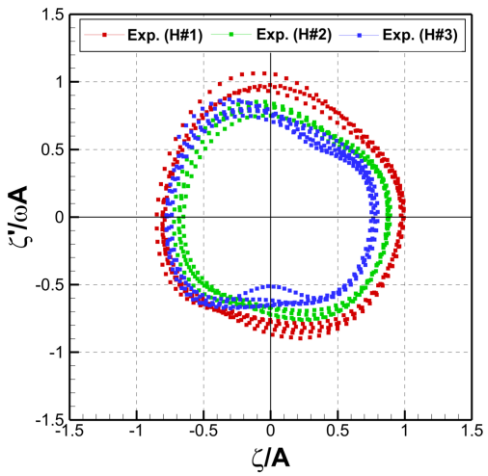

Fig. 4. Phase portrait of surface motion inside the OWC chamber under various wave height conditions (ω=1000 rpm).

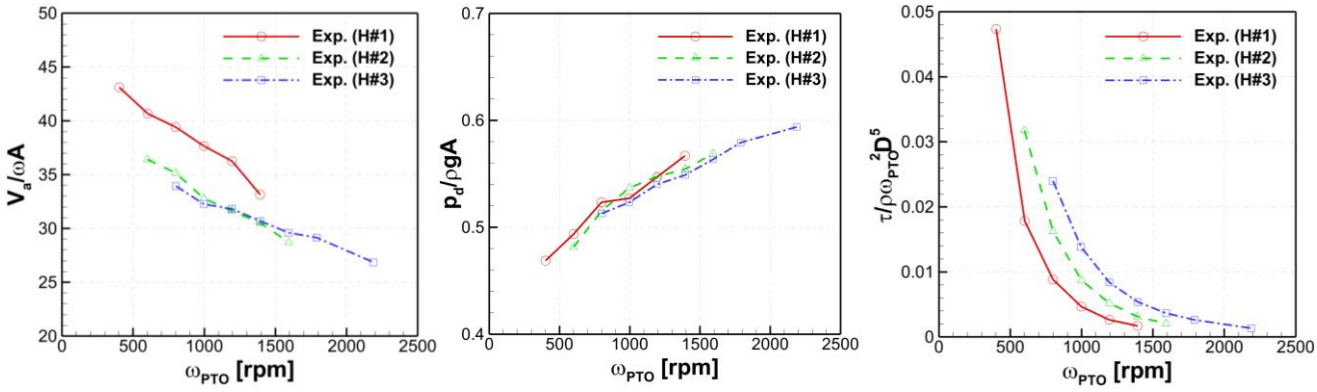

(a) Airflow velocity (b) Pressure drop (c) Mechanical torque

Fig. 5. Experimental measurements of the OWC chamber and air turbine under various wave heights and turbine's rotational speeds.

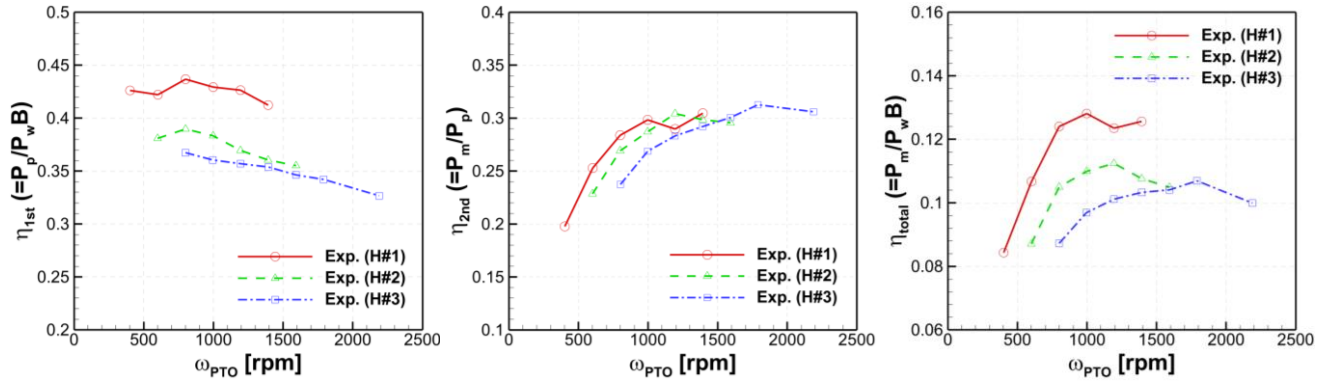

(a) Primary efficiency (chamber) (b) Secondary efficiency (turbine) (c) Total efficiency

Fig. 6. Energy conversion efficiency of the turbine-integrated OWC chamber under various wave heights and turbine's rotational speeds.

This measurement is related to the amount and pressure of air flowing out under the skirt of the chamber exposed to the atmosphere when the lower trough of the incident wave is placed in front of the chamber. Here, the draft of the skirt structure is 65 mm, and the wave trough of the H#3 condition is about 70 mm. Therefore, it can be seen that negative surface motion increased as the negative pressure inside the chamber decreased during inflow conditions. The phase portrait was introduced to analyze the behavioral characteristics of the absorbing wave energy at the OWC chamber. Fig. 4 shows the phase portrait of the internal water surface motion under the turbine rotation speed of 1000 rpm, and the experimental results of the three wave height conditions are compared under the quasi-steady state based on the time-series data. Here, the x- and y-axis are the position and velocity of the internal water surface, respectively. From the trajectory of the phase portrait, the internal water surface motion shows the asymmetric behavior between the discharge and intake flow conditions in terms of position and velocity. In conditions H#1-2, it is observed that the trajectory of the phase portrait narrows as the wave height increases. This phenomenon indicates a decrease in the energy conversion efficiency of the OWC system due to the nonlinearity of the chamber's internal pressure, affecting both the magnitude of internal water surface motion and the generated airflow rate as the wave height increases. In condition H#3, where the skirt is exposed to the atmosphere, a trajectory transformation is observed as the pressure inside the chamber is discharged through the skirt. It can be seen that the pressure discharge from the chamber interior directly impacts the primary energy conversion performance.

Fig. 5 shows the mean airflow velocity (V_a) estimated by the measured surface motion, mean pressure, and mean mechanical torque acting on the air turbine. As shown in Fig. 5(a), the airflow velocity shows a similar tendency to the chamber exposure effect under the H#3 condition. The restricted water column motion directly affects the airflow velocity under the large wave condition. However, the pressure drop shows the same tendency regardless of the wave height variation under the turbine's various rotation speeds. Fig. 5(c) shows the mean mechanical torque acting on the air turbine by the airflow. In the torque measurement results, the effect of the wave height was clearly distinguished. For the same rotation speed, higher amplitude waves result in higher torque.

Fig. 6 shows the energy conversion efficiency of the turbine-integrated OWC chamber model. Each figure represents the conversion efficiency at each stage of energy conversion. In the experimental model, energy is sequentially converted from incident wave energy flux (P_w) to the chamber's pneumatic power (P_p) and to the turbine's mechanical power (P_m). P_w, P_p, and P_m are defined as follows.

$$P_w = Ec_g = \frac{1}{8}\rho g H^2 \frac{\omega}{k}\left(1 + \frac{2kh}{\sinh 2kh}\right) \quad (1)$$

$$P_p = \frac{1}{T}\int_0^T Q(t) \cdot p_d(t)\, dt \tag{2}$$

$$P_m = \frac{1}{T}\int_0^T \omega(t) \cdot \tau(t)\, dt \tag{3}$$

where, c_g corresponds to the wave group velocity.

The primary energy conversion efficiency (η_{1st}) gradually decreased as the turbine rotation speed increased, and the decrease was large at high incident waves. On the other hand, the secondary energy conversion efficiency (η_{2nd}) gradually increased with the increase of the turbine rotational speed and showed a tendency to converge. The total energy conversion efficiency (η_{total}) including primary and secondary showed a parabolic shape with an optimum point depending on the rotational speed of the turbine. This parabolic tendency is similar to the OWC chamber performance depending on radiation pressure from the PTO system [6]. Furthermore, the optimum rotational speed tended to increase as the incident wave height increased.

IV. CONCLUDING REMARKS

This study conducted model tests for the turbine-integrated OWC chamber in the two-dimensional wave tank. The nonlinear and asymmetric water column movements according to the incident wave height can be confirmed from the experimental observation. These hydrodynamic aspects directly affect the energy conversion performance of the air turbine and the OWC chamber. During high waves, air may flow into the exposed skirt as well as the air duct, which affects the energy conversion performance of the chamber and air turbine. In addition, the turbine-integrated OWC chamber shows the opposite pneumatic and mechanical energy conversion characteristics. It was confirmed that the optimal operating condition dependent on the incident wave height existed in terms of the total energy conversion performance of the entire system. In future research, the energy conversion process of the OWC wave energy converter will be investigated in detail by expanding the experimental conditions considering various regular and irregular waves and the operating conditions of the PTO system. Furthermore, the numerical method for fully-coupled energy conversion of the OWC wave energy converter will be verified using experimental data.

REFERENCES

[1] A. F. Falcao, J. C. Henriques, "Oscillating-water-column wave energy converters and air turbines: A review," *Renewable Energy*, vol. 83, pp. 1391-1424, 2016. DOI: 10.1016/j.renene.2015.07.086, [Online].

[2] J.-S. Kim, B. W. Nam, K.-H. Kim, S. Park, S.-H. Shin, K. Hong, "A numerical study on hydrodynamic performance of an inclined OWC wave energy converter with nonlinear turbine-chamber interaction based on 3D potential flow," Journal of Marine Science and Engineering, vol 8, no. 3, p. 176, 2020. DOI: 10.3390/jmse8030176, [Online].

[3] J.-S. Kim, "Numerical study on fully coupled hydrodynamic energy conversion problem of OWC-WEC system," Ph.D. dissertation, Korea Maritime and Ocean University, South Korea, 2021.

[4] Z. Liu, C. Xu, N. Qu, Y. Cui, K. Kim, "Overall performance evaluation of a model-scale OWC wave energy converter," Renewable Energy, vol. 149, pp. 1325-1338, 2020. DOI: 10.1016/j.renene.2019.10.126, [Online].

[5] Z. Liu, C. Xu, K. Kim, "Overall performance of a model OWC system under the free-spinning mode: An experimental study," Ocean Engineering, vol. 227, no. 108890, 2021. DOI: 10.1016/j.oceaneng.2021.108890, [Online].

[6] J.-S. Kim, K.-H. Kim, J. Park, S. Park, S.-H. Shin, "A numerical study on hydrodynamic energy conversions of OWC-WEC with the linear decomposition method under irregular waves," Energies, vol. 14(6), no. 1522, 2021. DOI: 10.3390/en14061522, [Online].